A numerical model for the transport of a boulder by tsunami

Fumihiko Imamura

Kazuhisa Goto

(Corresponding author)

Shigeki Ohkubo

Disaster Control Research Center, Tohoku University, 6-6-11 Aoba, Sendai, 980-8579 Japan

E-mail: kgoto@tsunami2.civil.tohoku.ac.jp

Submitted to

Journal of Geophysical Research-Oceans

INDEX TERMS: 4203 Analytical modeling and laboratory experiments, 4255 Numerical modeling (0545, 0560), 4558 Sediment transport (1862), 4564 Tsunamis and storm surges

Keywords: tsunami, boulder, sediment, hydraulic experiment, numerical model

Abstract

We have conducted hydraulic experiments in an open channel with cubic and rectangular shaped solid blocks on the slope for investigating the boulder transport process by tsunami. In our experiments, the block was mainly seen to be transported by a bore due to rolling or saltation rather than by sliding. Previous models for the boulder transport by tsunamis assumed sliding as a mode of transport for the boulder. Therefore, these models underestimated the distance of the boulder moved by the tsunami when it was transported due to rolling or saltation. In this study, we have developed a practical model for the transport of a boulder by tsunami, which takes into account the various transport modes. We introduce an empirical variable coefficient of friction by assuming that the coefficient decreases with decrease in ground contact time when the block was transported by rolling or saltation. With the aid of this parameter, the model can explain various modes of transport, i.e., sliding, rolling, and saltation, and reproduces the experimental results well. We further applied this improved model to a tsunami boulder at Inoda area in Ishigaki Island, Japan, which was transported by the 1771 Meiwa tsunami. The calculated distance of transport of the boulder was approximately 650 m, which is consistent with the description in the historical document. Based on our calculations, we estimated hydraulic values of the tsunamis. Estimation of such hydraulic values is important for understanding the behavior and power of the historical tsunamis, besides aiding future disaster mitigation efforts.

1. Introduction

It has been reported that large tsunami waves transport huge boulders of lengths of a few meters [e. g., *Kato and Kimura*, 1983]. A typical example would be the hundreds of reef boulders (>300 in number) scattered along the shore and on land of Ishigaki Island, Japan (Figure 1) [e.g., *Kato and Kimura*, 1983; *Nakata and Kawana*, 1993]. The largest of these boulders weighed 700 t [*Kato and Kimura*, 1983]. These reef boulders, called "tsunami-*ishi* (stone)" in Japanese, are thought to have been transported by the 1771 Meiwa tsunami, which, according to historical documents, had wave heights of ~30 m. Moreover, abundant boulders of coral fragments having lengths of few meters were transported by the tsunamis associated with the 1883 Krakatau volcanic eruption [*Simkin and Fiske*, 1983] and the 2004 Indian Ocean tsunami [*Goto et al.,* 2007. accepted]. Similarly, boulders transported by possible historic or prehistoric tsunami have been reported from the coastal areas of Japan, Australia, Italy, the United States (Hawaii), Spain, and Portugal [e. g., *Noji et al*., 1993; *Mastronuzzi and Sanso*, 2000; *Nott*, 2000, 2004; *Noormets et al*., 2002, 2004; *Scheffers and Kelletat*, 2005; *Whelan and Kelletat*, 2005; *Goff et al*., 2006], although their origin is still debated [*Nott*, 2000; *Noormets et al*., 2004].

Damage due to tsunamis is mainly related to its hydraulic force and the current velocity rather than to the inundation depth or the wave height [e. g., *Noji et al*., 1993]. However, in general, hydraulic force and the current velocity are difficult to estimate from field observations. Even when a field survey is conducted immediately after a tsunami event, many data dealing with the inundation depth, area and the wave heights are collected, very few data on the hydraulic force or current velocity are available. The ability of a tsunami to transport boulders is closely related to the hydraulic force of the tsunami and hence, the estimation of the hydraulic force and current velocity are necessary to understand the transport of these boulders. For example, the minimum current velocity or wave height necessary for moving a boulder can be theoretically estimated from the weight and shape of the boulder [e. g., *Nott*, 2003; *Noormets et al*., 2004]. However, estimations of the time series of the hydraulic force and current velocity as well as their maximum values are important for understanding the behavior and power of the historical tsunamis and to aid in future disaster mitigation efforts. Therefore, numerical modeling is required to understand in detail the transport process and variations of the hydraulic force during the transport of boulders. A numerical model of the transport of a boulder was developed by *Noji et al*. [1993] and was extended to two-dimensions by *Imamura et al*. [2001]. However, the model assumed sliding as the only transport mode, although boulders can be transported due to rolling or saltation also, depending on the shape and hydraulic force of the tsunamis [*Goto et al*., 2006]. When the boulder was transported due to rolling or saltation, it would probably be transported further than for the case of sliding, because of the reduced friction and the effect of centrifugal force.

In this study, we have conducted hydraulic experiments to observe the modes of transport of the boulder. Consequently, we improve the model by including rolling and saltation also for the transport, besides the sliding. We apply this improved model to an event at Inoda area, Ishigaki Island, Japan due to the 1771 Meiwa tsunami.

2. Physical method for hydraulic experiment

At the Disaster Control Research Center in Tohoku University, hydraulic experiments were conducted in a water tank, 10 m long by 30 cm wide, and having a flat bottom (Figure 2). A gate located 300 cm from the upstream end of the tank confines water in a storage tank, and acts as a wave generator. A bore is generated by rapid opening of this gate. The initial depth of water at the downstream side of the gate was 1.2 cm.

A flat slope with a varying gradient was used to simulate the shore, and was kept at a distance of 250 cm downstream from the gate, where the bore becomes steady and stable height. The gradient of the slope was set at 1:10, because bottom friction and gravity forces are effective in this setting, and thus it suits for validation of the model (see also appendix 1). The surfaces of the floor and the slope are smooth and impermeable. The current velocity of the bore can be varied by adjusting the depth of water in the storage tank, which was set at 15, 20, 25, and 30 cm, respectively. For these depths, the bore was found to have reached approximately 150, 215, 280, and 335 cm from the bottom of the slope.

The bore which was generated, runs up the slope, reaches a maximum inundation level, and then flows back towards the upstream side as backwash current. The time series of the current velocity was measured at the initial position of the block and 100 cm above the flat floor with a temporal resolution of 0.001 s (Figure 3). The backwash current was dewatered through a drainage gate at the upstream end of the storage tank (Figure 2). Using this system, we can measure the process by which the block is transported by a single bore.

We have used two coral and silicate cubic blocks each (blocks A, B, C, and D-1) for the hydraulic experiment (Table 1). The block was set at the bottom of the slope (Figures 2 and 4a). The hydraulic experiments were conducted 5 times for each case and were recorded by using a video camera in order to analyze the transport process and the path of the block.

We have also investigated the behavior of a solid rectangular block, because its motion might be different from that of a cube shaped block. We used silicate rock to prepare three different blocks, where the ratios between the long and short axes were 1:1, 1:2, and 1:3, respectively (Table. 1, D-1, D-2, and D-3). The behavior of the block may vary depending on the initial orientation of the long axis against the direction of the current, since the projected area of the block against the current would vary and consequently the drag force acting on the block would be different. Therefore, we set the initial orientation of the long axis of the block both perpendicular and parallel to the direction of the current (Figure 4b). The water levels in the storage tank were kept at 15, 20, 25, and 30 cm and hydraulic experiments were performed five times in each case.

3. Experimental results

3.1. Motion of the cubic block and the rectangular solid block

When the bore front hits the block, the block starts moving up the slope and stops finally at the location in accordance with the decreasing current velocity (Figure 4a). In our experiment, the cubic block was found to have transported mainly due to rolling or saltation rather than sliding from each case. However, when the current velocity decreases, the block was transported by sliding. The block was then moved in the downstream direction by the wave backwash, and finally comes to a stop in accordance with the decreasing backwash current velocity (Figure 4a). Through the backwash process, the block was mainly found to have been transported by sliding or rolling. The maximum measured displacement attained and the final position of the block where it came to rest is shown for each case in Figure 5. These were found to increase with increasing volume of water in the storage tank, which in turn increases the current velocity.

When we set the orientation of the long axis of the solid rectangular block perpendicular to the current, the block was found to have been transported mainly due to rolling or saltation by the current to sustain its original orientation (Figure 4b). In this case, the average maximum displacement and the location where it comes to rest were found to be within the range of the cubic block (Figure 6a). On the other hand, when we set the orientation of the long axis of the block parallel to the current, the block was found to have been rotated suddenly when the bore front fell on the block and changed its orientation perpendicular to the direction of the current (Figure 4b). Consequently, it was found to have been transported up the slope, sustaining this orientation perpendicular to that of the current direction (Figure 4b). In this case, the maximum displacement and the position where the block came to rest were found to be significantly shorter compared to those for the cubic block (Figure 6b).

3.2 Interpretation of the block motion in the experiment

Here, we discuss the major characteristics of the block motion in the physical experiment on the uniform slope. Theoretical explanation and the numerical model of the block transport by tsunami are introduced in chapter 4. As stated above, the cubic block was found to have been transported mainly due to rolling or saltation rather than sliding from each case. Although previous studies indicate that block sliding is the preferred mode of incipient motion [*Walder et al.*, 2006], the block does not necessarily start the motion of sliding, and incipient motion would vary depending on some factors such as hydraulic force and block shape. Our result in the experiment indicates that the initial impact of the bore is strong, and the block was flicked by the bore to move rolling or saltate, which, consequently, generate the centrifugal force. These characteristics are to be modeled in the coefficient of friction in chapter 4.3. On the other hand, through the backwash process, the block was mainly found to have been transported by sliding or rolling. This is because the current velocity of the backwash was weaker than the run-up current (Figure 3).

When the water level in the storage tank was 15 cm, the cubic block was found not to move down the slope due to the backwash, because the hydraulic force is weak to move the block in this case. But, when the water level in the storage tank was 30 cm and on using blocks A and B, it was found to move down the slope due to the strong backwash. Furthermore, the maximum displacements and the positions where the blocks finally came to rest for the coral rocks (Blocks A and B) were found to be greater than the silicate rocks (Blocks C and D-1) of similar size. These results are due to the smaller densities of the blocks A and B and as a result, the hydraulic force becomes higher. These results are consistent with the previous experiments and theoretical analysis on block motion using blocks with different densities [e.g., *Watts*, 1998, 2000; *Nott*, 2003].

When we set the orientation of the long axis of the solid rectangular block perpendicular to the current, the average maximum displacement and the location where it comes to rest were found to be within the range of the cubic block. This is because the hydraulic force acting per unit-projected area of the block in the opposite direction to the current is similar to that for the cubic block for this case. On the other hand, when we set the orientation of the long axis of the block parallel to the current, the maximum displacement and the position where the block came to rest were found to be significantly shorter compared to those for the cubic block (Figure 6b). Because part of the hydraulic force was used for rotating the block, the force available to transport the block becomes weaker, and consequently the distance transported in this case becomes shorter than that of the cubic block.

4. Development of the model - Boulder Transport by the Tsunami (BTT-model)

4.1. Numerical model of the wave current for hydraulic experiment

Before the calculation of the block transport, an accurate reproduction of the wave current is required. Shallow-water theory was used for numerical calculation of the tsunami propagation in the shallow region and the run-up.

$$\frac{\partial \eta}{\partial t} + \frac{\partial M}{\partial x} = 0 \tag{4.1}$$

$$\frac{\partial M}{\partial t} + \frac{\partial}{\partial x}\left(\frac{M^2}{D}\right) + gD\frac{\partial \eta}{\partial x} + \frac{gn^2}{D^{7/3}} M|M| = 0 \tag{4.2}$$

where η is the vertical displacement of the water surface above the still-water surface, M is the discharge flux in the x direction, D is total water depth (= $h + \eta$), and n is Manning's roughness coefficient. Manning's roughness coefficient was estimated to be 0.0125 for the experiment. For the calculation of the open channel, the coefficients of static and dynamic friction were estimated to be in the ranges of 0.65 to 0.8 and 0.5 to 0.7, respectively. These values are estimated through our experiment and are closer to those at the coastal area of Ishigaki Island (0.75 and 0.71 for the coefficients of static and dynamic friction, respectively, according to *Imamura et al*., 2001). The staggered leap-frog method, which is a finite-difference method, was used to solve these equations numerically [*Goto et al*., 1997, *Kotani et al*. 1998]. As shown in Figure 3, although the calculated current velocity is slightly overestimated at the backwash current, it agrees well with the measured value from the experiment.

Experimental results must be interpreted in light of the principle of similarity in order to apply for the case of a real scale tsunami event. In the field case (the 1771 Meiwa tsunami case), there is no field observation data of the current velocity, which in turn indicates that we can not estimate the Shields, Froude and Reynolds numbers directly from the field data. Thus, we estimated these numbers using the numerical result by *Imamura et al*. [2001]. This numerical result well explains the wave height and inundation area of the tsunami estimated by *Kawana* [2000]. Current velocity of the 1771 Meiwa tsunami is computed as less than 15 m/s at Inoda [*Imamura et al*., 2001]. Considering that the current velocity of the 2004 Indian Ocean tsunami is approximately 2~5 m/s at Banda Aceh, Indonesia [*Fritz et al*., 2006] and 6~8 m/s along the coastline at Khao Lak, Thailand [*Matsutomi et al*.,2006], estimated current velocity for the 1771 Meiwa tsunami is plausible, because the scale (e.g., wave height) of the 1771 Meiwa tsunami at Inoda [*Kawana,* 2000; *Imamura et al*., 2001] is several times larger than that of the 2004 Indian Ocean tsunami at Banda Aceh and Khao Lak.

Based on these assumptions, the Shields number of the 1771 Meiwa tsunami is estimated as 5-8 [*Imamura et al*., 2001]. This is similar in range to that of the 1960 Chile tsunami at the Japanese coast (less than 10), which was estimated from aerial photographs [*Takahashi et al.*, 2000]. The Shields number for our experiment was approximately 4 to 10, and the number for the hydraulic experiment was within a range similar to that of real-scale tsunamis. The Froude number for our experiment was approximately <1.3, whereas that is <1.0 for the 1771 Meiwa tsunami.

When we use the length of the block as representative length, the Reynolds numbers for the experiment is estimated as order of 10^4 and the 1771 Meiwa tsunami is estimated as order of 10^7. Both are large Reynolds numbers and indicate fully developed turbulent flow. It is well known the one cannot match both Froude and Reynolds numbers in the same scaling experiment, and agreement of the Shield and Froude numbers are more important in this study. Based on these observations, our model developed below can be applied to real scale tsunami events.

4.2. Basic model

External forces, including those produced by the tsunami wave current, acting on the block are represented by the hydraulic force F_m, the frictional force at the bottom F_b, and the component of the gravitational force F_g along the slope (Figure 7a) [*Noji et al.*, 1993].

$$\rho_s V \ddot{X} = F_m - F_b - F_g \quad (4\text{-}3)$$

where ρ_s is the density of the block, V is the volume of the block, and X is the position of the block in the x-direction. F_m represents the sum of the forces of drag and inertia [*Noji et al.*, 1993].

$$F_m = C_D \frac{1}{2}\rho_f A(U - \dot{X})|U - \dot{X}| + C_M \rho_f V \dot{U} - (C_M - 1)\rho_f V \ddot{X} \tag{4-4}$$

where U is the current velocity at the position of the block, A is the projected area of the block against the current, and C_D and C_M are coefficients of drag and mass, respectively. F_b and F_g are represented as follows.

$$F_b = \mu(\rho_s - \rho_f)Vg\cos\theta \frac{\dot{X}}{|\dot{X}|} \tag{4-5}$$

$$F_g = (\rho_s - \rho_f)Vg\sin\theta \tag{4-6}$$

where θ is the angle of the slope at the position of the block and μ is the coefficient of friction.

Based on the hydraulic experiment, *Noji et al.* [1993] proposed empirical equations to estimate values for C_D and C_M as follows.

$$Log_{10}C_D = \alpha - 1.6Log_{10}F_r \tag{4-7}$$

$$\alpha = \begin{Bmatrix} 0.13 & for\ h/H < 1.2 \\ 0.28 - 0.1h/H & for\ 1.2 \le h/H < 3.6 \\ -0.08 & for\ 3.6 \le h/H \end{Bmatrix} \tag{4-8}$$

when C_D<1.6, then C_D =1.6.

$$C_M = 1.15 + 1.15\tanh\{(-2.0 + 2.5h/H)\pi\} \quad for\ h/H < 1.0 \tag{4-9}$$

where F_r is Froude number, h is depth of water at the position of the block, and H is height of the block. The interaction between the block and the fluid is taken into consideration in this model [*Noji et al.*, 1993]. Therefore, the force of resistance of the block against the current should be considered in equation (4-2), which can be written as follows.

$$\frac{\partial M}{\partial t}+\frac{\partial}{\partial x}\left(\frac{M^2}{D}\right)+gD\frac{\partial \eta}{\partial x}+\frac{gn^2}{D^{7/3}}M|M|+\frac{F_m}{\Delta x}=0 \qquad (4\text{-}10)$$

where Δx is the spatial interval of the grid. In this model, C_D and C_M vary depending on the relative depth (h/H) at the position of the block. Similar experimentally derived drag and added mass coefficients for solid blocks were proposed [e.g., *Watts*, 1998, 2000]. However, although these models are a rigorous one, the current motion is very complex around the block and it is then difficult to estimate the current velocity. Therefore, error in the drag force, which is proportional to the square of current velocity, becomes significant [*Imamura et al.*, 2001]. Hence, in this study, we do not use equations (4-7) to (4-10). Coefficient of drag C_D would be constant under the 10^4 order of the Reynolds number and we chose the C_D based on the relationship to the Reynolds number [e.g., *Hoerner*, 1965: *Julien*, 1995]. We have fixed C_D and C_M values to be 1.05 and 1.67, respectively, and used the current velocity in the absence of the block for our calculation.

4.3. Adoption of variable coefficient of friction

The coefficient of friction μ remained a constant when the block was transported by sliding, but it is possible that the block can also be transported due to rolling or saltation, depending on its shape and the hydraulic force of the tsunami (Figure 7). In fact, the block was found to have been transported mainly due to rolling or saltation in our hydraulic experiments. It is possible to make separate models for each modes of transport of the block, but they change continuously from sliding to rolling or saltation following the variation in the hydraulic force. Therefore, it is important to incorporate this continuous variation of the modes of transport of the block into one single model.

In order to make a practical model, we introduce a variable coefficient of friction $\mu(t)$ by assuming that it decreases as a result of reduced ground contact time when the block was transported due to rolling or saltation (Figure 7). When we transform the equations (4-3) and (4-5), $\mu(t)$ can be expressed as follows.

$$\mu(t) = \frac{F_m - F_g - \rho_s d^3 \ddot{X}}{(\rho_s - \rho_f) d^3 g \cos\theta} \tag{4-11}$$

In order to calculate the right hand side of equation (4-11), the position, velocity, and acceleration of the block, and the current velocity and acceleration at the position of the block at each instant are required, and we make use of video images to obtain these values. We measured the position of the block every 0.6 [s] intervals and estimated the velocity and acceleration of the block. Acceleration was calculated using the variation in the measured current velocity at every 0.6 [s] intervals.

Based on our observation, it is possible to assume that the trajectory of barycenter of the block shows repeated arc like shapes (Figure 7b). The block starts rolling or saltate due to the centrifugal force when the angular velocity increases. Therefore, we assume that the block undergoes rolling or saltation when the centrifugal force exceeds the weight of the block in water (Figure 7b).

$$(\rho_s d^3) d' \omega^2 > \left\{ (\rho_s - \rho_f) d^3 \right\} g \cos\theta \tag{4-12}$$

where *d'* is a radius of the trajectory of barycenter of the block. The block would be transported due to sliding when the left hand side of equation (4-12) becomes smaller than the right hand side, whereas the block would be transported due to rolling or saltation when the left hand side is larger.

We adopt a parameter β which indicates the degree of contact between the block and the floor. β is represented by the ratio of the left hand side to the right hand side of equation (4-12). When we assume $d' \propto d$, $\omega \propto \ddot{X}/d$, and cos θ=1, equation (4-12) is expressed as follow.

$$\frac{(\rho_s d^3) d' \omega^2}{\{(\rho_s - \rho_f) d^3\} g \cos\theta} \propto \frac{\dot{X}^2}{(1 - \rho_f / \rho_s)} = \beta^2 \qquad (4\text{-}13)$$

More precisely, β includes the effect of the force of lift. Based on the curve fit analysis of our experimental results (Figure 8), the relationship between $\mu(t)$ and β can be empirically expressed as follow.

$$\frac{\mu(t)}{\mu_0} = \frac{2.2}{\beta^2 + 2.2} \qquad (4\text{-}14)$$

where μ_0 is the coefficient of dynamic friction during sliding. In this analysis, we do not consider the physical error of equation (4.14) and used average curve fit value as representative, because block acceleration errors are larger than the physical error. According to equation (4-14), $\mu(t) = \mu_0$ when $\beta = 0$, which indicates that the block moved as a result of sliding. When the current velocity increases or density of the block decreases, β becomes larger and thus $\mu(t)$, smaller. This indicates reduction in the ground contact time, and the block becomes more movable compared to sliding (Figure 7b), representing the transport modes due to rolling or saltation.

4.4. Expansion of the model for the case of the rectangular solid block

In this section, we extend the model to include a rectangular solid block. As stated above, the rectangular solid block was transported mainly with its long axis oriented perpendicular to the direction of the current. In this case, the equation of motion for the rectangular solid block with short axis d and long axis kd can be expressed as follows.

$$\rho_s (kd^3)\ddot{X} = C_D \frac{1}{2}\rho_f (U-\dot{X})|U-\dot{X}|(kd^2) + C_M \rho_f \dot{U}(kd^3) - (C_M - 1)\rho_f \ddot{X}(kd^3) - kF_b - kF_g \qquad (4\text{-}15)$$

Each term in equation (4-15) were multiplied by k. In the absence of k, equation (4-15) and equation (4-3) are the same. Therefore, the motion of the rectangular solid block calculated using this equation corresponds to the motion of the cubic block. This is consistent with experimental results, where the initial orientation of the long axis of the block when kept perpendicular to the current, it was found that the maximum displacement and the final position where the block was found to have stopped were almost similar for the cubic and rectangular solid blocks (Figure 6a). But, the maximum displacement for the rectangular solid block was found to be shorter than that for the cubic block, when we set the initial orientation of the long axis of the block parallel to the current. Therefore, equation (4-15) would be inapplicable in this case and further improvement of the model, which would take into account the initial rotational motion of the block when it meets the bore front, is warranted.

4.5. Numerical results for the open channel

Overall, the numerical results obtained by using a constant coefficient of friction were found to underestimate the experimental results (Figure 5). Especially, it significantly underestimates when the current velocity was fast or the density of the block, smaller. According to our observations, the block was moved mainly as a result of rolling or saltation with increasing current velocity or decreasing density of the block. Therefore, when we assume a constant coefficient of friction, with sliding, the friction is overestimated and the block would be harder to move. On the other hand, the numerical results obtained by using a variable coefficient of friction were within the error range compared to the experimental results (Figure 5). These indicate that our model reproduces well the variation due to different transport modes of rolling, saltation or sliding. Although we made the model based on the hydraulic experiment with steep slope (1:10), our model is also applicable to the flat or mild slope case (see appendix 1).

Hence, this newly improved model reproduces the experimental results better, but these results must be interpreted in light of the principle of similarity in order to apply for the case of a real scale tsunami event. As stated above, the Shields and Froude numbers for our experiment were in good agreement with the field scale tsunamis. Therefore, our model can be applied to real scale tsunami events. In the next chapter, we apply this model, hereafter denoted by the model for Boulder Transport by the Tsunami (BTT-model), to the real scenario of boulder transport by tsunami.

5. Application of the model to the 1771 Meiwa tsunami event

5.1. The 1771 Meiwa tsunami

On 24^{th} of April 1771, a tsunami called the 1771 Meiwa tsunami, and reaching heights of up to 30 m, attacked to the Yaeyama and Miyako Island chains of Japan (Figure 9) and killed more than 12,000 people [*Nakata and Kawana*, 1995]. According to historical documents, more than 300 coral boulders having lengths of few meters were transported by this tsunami and deposited around the coastal area of the Yaeyama and Miyako Island chains (Figure 1) [*Nakata and Kawana*, 1995]. No successful research to reproduce the movement of tsunami boulder in Ishigaki Island in the case of the 1771 Meiwa tsunami has been carried out so far. It is important to note that many boulders observed in the coastal area and on land in these islands could have been possibly removed before by tsunami event(s) prior to the 1771 event [*Nakata and Kawana*, 1995; *Kawana*, 2000]. Therefore, for most of these boulders, it is difficult to identify their original position just before the 1771 tsunami using geological methods. Nevertheless, *Kawana* [2000] estimated the original locations of some boulders at Yasura, Inoda, and Ohama areas in the Ishigaki Island (Figure 9) based on the description in historical documents. For example, the boulder at Inoda area, which is composed of coral and having a density of 1.5 g/cm^3 and dimensions of approximately 5.2×5.2×6.0 m (Figure 1b), was a famous rock before the 1771 tsunami and was known as “Amatariya-suuari”. It was originally located approximately 327 m (“3 chou” in old Japanese unit of distance) from the shoreline, known as “amatariya”, and was transported landward later by the 1771 Meiwa tsunami, and deposited approximately 218 m (“2 chou”) inland from the shoreline [*Kawana*, 2000].

The boulder at Inoda area is suitable for validating our model based on the following reasons: 1) there is an available historical document which describes that the boulder was transported by the 1771 Meiwa Yaeyama tsunami, 2) the bathymetry around the Inoda area is simple for comparing with other areas, 3) the approximate original position was estimated [*Kawana*, 2000], 4) the detachment and emplacement processes probably need not be take into account because the boulder could have been already detached and emplaced before 1771

[*Kawana*, 2000], 5) the effect of collisions and the shielding effect among the boulders are negligible because only few huge boulders were transported to the Inoda area by the 1771 tsunami, and 6) the boulder was deposited approximately 200 m inland from the shoreline and thus it has been never moved by high waves generated as a result of typhoons after the 1771 tsunami. Therefore, in this study, we investigate the transport process of the boulder at Inoda area using the BTT-model.

5.2. Numerical simulation of the 1771 Meiwa tsunami

To simulate tsunami propagation in the open sea, we use a linear equation to describe shallow-water waves, and for the coastal zone and the inundation area, a nonlinear equation in cartesian coordinates was used [*Goto et al*., 1997]. Although several models of tsunami source have been proposed for the 1771 Meiwa event [*Imamura et al*., 2001; *Nakamura*, 2006], we use the model proposed by *Imamura et al*. [2001]. This model assumes the generation of landslides along with fault displacement, and the estimated [*Nakata and Kawana,* 1995; *Kawana*, 2000] tsunami run up heights were reproduced well by this model [*Imamura et al*., 2001]. The spatial resolution of the grid for Inoda region is 16.7 m and the time step is 0.1s.

In the two dimensional BTT model, the equation of motion for the boulder can be separated into the x and y components.

$$\rho_s Vx = F_{mx} - F_{bx} - F_{gx} \tag{5-1}$$

$$\rho_s Vy = F_{my} - F_{by} - F_{gy} \tag{5-2}$$

The hydraulic force F_m in x and y directions can be expressed as follows.

$$F_{mx} = C_D \frac{1}{2} \rho_f (u - x)\sqrt{(u - x)^2 + (v - y)^2} A + C_M \rho_f uV - (C_M - 1)\rho_f xV \qquad (5\text{-}3)$$

$$F_{my} = C_D \frac{1}{2} \rho_f (v - y)\sqrt{(u - x)^2 + (v - y)^2} A + C_M \rho_f vV - (C_M - 1)\rho_f vV \qquad (5\text{-}4)$$

where *u* and *v* are the x and y components of the current velocity at the location of the boulder. We have fixed C_D and C_M values to be typical 1.05 and 1.67 [e.g., *Hoerner*, 1965] in both x- and y- directions, respectively (see appendix 2). The Manning's roughness coefficient was 0.025, which value is normally used for the coastal area [e.g., *Linsley and Franzini*, 1979; *Kotani et al*., 1998].

Based on the work by *Kawana* [2000], we assume the original locations of the boulder (locations P1 to P4 in Figure 10), to be approximately 327 m offshore from the shoreline. Besides, we also assume rectangular solid boulder, and the projected area of the boulder against the current was assumed to be 5.2×6.0 m.

5.3. Results and discussion

The first tsunami wave arrived at the area under investigation approximately 800 s after the generation of the tsunami (Figure 11). The tsunami wave current inundated ~800 m inland from the shoreline at Inoda area (Figure 10). The maximum wave height was approximately 19 m according to our calculation (Figure 11). The bathymetry and topography around this area are almost flat at an elevation of 20 m. Thus, the incident direction of the tsunami wave current is almost uniform until this level (Figure 10). But, there are V-shaped valleys above 20 m and the current direction changed along these valleys.

The boulder was found to have been transported towards the northwest by the first and second wave currents and consequently moved shoreward slightly due to the backwash. The boulder was not moved by subsequent waves, because the boulder came to rest on land as a result of the first and second waves and the hydraulic force of subsequent waves were not strong enough to move the boulder from this position.

The displacement of the boulder using a variable coefficient of friction (μ) was found to be 650 m approximately, and is in good agreement with the estimation of *Kawana* [2000], whereas those obtained when μ was kept constant didn't agree well (Figure 10). The trajectory and distance moved by the boulder were different depending on the initial position of the boulder. This is because the direction of the current and velocity differ from location to location depending on the bathymetry. When we assumed the original position of the boulder to be at P2 and we use a variable coefficient of friction, the final position of the boulder is very close to the present position (Figure 10).

Based on our calculations, the maximum velocities of the current and the boulder in this area was estimated to be at 15.1 m/s and 12.5 m/s, respectively, and the maximum hydraulic force was estimated to be 1.16×10^{6} N. The boulder came to a stop when the current velocity became lower than 2 m/s. The estimation of these hydraulic values is important for understanding the behavior of such historical tsunamis and would aid in preparations against future events.

6. Limitations of the BTT model and proposed improvements

In this study, we have improved the boulder transport model to be applicable for the continuous change in the mode of transport from sliding to rolling and saltation. The estimated displacement of the boulder at Inoda area using the BTT-model was found to be well consistent with the historical description. Therefore, we consider that this model can be applied to a real scale event of boulder transport by the tsunami. Using this model, it is possible to estimate the behavior of the boulder under varying hydraulic force of the tsunami in detail. For example, the 2004 Indian Ocean tsunami transported large reef boulders, up to 4 m in length, landward at Pakarang Cape, Thailand [*Goto et al*., 2006]. The field observations suggest that the first, eastward-directed tsunami waves struck the reef rocks, which were originally located on the shallow sea bottom near the reef edge (300 to 600 m offshore), thereby transporting them shoreward [*Goto et al*., 2006]. In this case, the original and final positions of the boulders were well estimated, as are the tsunami wave height, inundation area, and topography. Therefore, the BTT-model can be applied for investigating the detailed transport process of the boulders.

Although boulders that are a few meters in length from possible historic or prehistoric tsunami have been reported at the coastal areas of countries that are at a high tsunami risk [e. g., *Noji et al*., 1993; *Nott*, 2000, 2004; *Mastronuzzi and Sanso*, 2000; *Noormets et al.*, 2002, 2004; *Whelan and Kelletat*, 2005; *Scheffers and Kelletat*, 2005; *Goff et al*., 2006], their origin with reference to storms is still under contention [*Nott*, 2000; *Noormets et al*., 2004]. *Nott* [2003] and *Noormets et al*. [2004] investigated whether the boulders can be moved by tsunamis or storm-generated high waves or swell waves. Although these approaches provide minimum current velocity or wave height necessary for moving the boulder, the actual velocity may be not so large and each of these waves might move the boulder in some cases. It is important to discuss the difference of the displacements of the boulders due to tsunamis and other waves, because this distance is critically related to the period of the wave. Our model can also be applied to the transport of boulders due to high waves generated by storms or by swell waves and thereby facilitating the testing of the processes behind such transport. This kind of analysis may provide important directions towards such debates.

The BTT-model has some limitations and requires the following further improvements.

1) The model is applicable for the case of a cubic boulder or a rectangular solid boulder, whose initial orientation of the long axis is perpendicular to the direction of the current. However, the displacement of the rectangular solid block varies depending on the initial orientation of the long axis. Our preliminary examination revealed that the initial orientation should be taken into account to the displacement of the rectangular solid shaped block, when the ratio between long and short axes of the block becomes larger than 2 [*Okada et al*., accepted]. However, even if we include the effect of initial orientation of the block in the model, in a real scenario such an estimate would be usually uncertain. Therefore, error bars indicative of this variation should be accounted for.

2) The shape of the boulder is also important in determining the displacement and behavior of the boulders due to the action by tsunamis. Our model assumed cubic or rectangular shaped solid boulder, but ellipsoidal or cone shaped boulders have also been also reported [*Goto et al*., 2006]. It is possible that these can be moved due to rolling easier compared to the cubic and rectangular solid boulders. Therefore, the shape of the boulder should also be included in the future model.

3) The BTT model does not include the detachment and emplacement processes of the boulder. For example, *Noormets et al*. [2004] estimated that the boulder deposited on the North Shore of Oahu, Hawaii was originally located on the edge of the shore platform, and that it was detached and emplaced on the platform by the swell wave or tsunami, thus transporting it further inland. They estimated that more than 60-70 % fracture is required to detach the boulder from the edge of the shore platform by a swell wave or tsunami [*Noormets et al.*, 2004]. The hydraulic force of the tsunami should weaken during the detachment and emplacement processes of the boulder. Therefore, estimation of the displacement due to transport using the BTT model may overestimate when such detachment and emplacement processes are not negligible.

4) At this moment, the BTT model is applicable only for the case of a single boulder. However, tsunamis usually transport numerous boulders at the same time [*Kato and Kimura*, 1983; *Simkin and Fiske*, 1983; *Goto et al*., 2007 accepted]. Moreover, it is reported that a number of tetrapods were transported inland by the 1983 Nihonkai-Chubu tsunami at Japan [*Noji et al.,* 1993]. In these cases, the effect of collisions among boulders and the shielding effect of boulders are not negligible. To clarify the transport processes for multiple boulders and tetrapods and hence be able to aid in the assessment of future tsunami risk, a numerical model for the transportation of multiple boulders, including the effect of collisions and shielding, should be developed.

7. Acknowledgments

We especially thank K. Okada for his support during our hydraulic experiment. This research was supported by a Grant-in-Aid for Scientific Research from the Japan Society for the Promotion of Science (experimental study for K. Goto: no. 17740331, and field and numerical studies for F. Imamura: no. 18201033). We thank two anonymous reviewers and J. Kirby for their valuable suggestions and comments.

8. References

Fritz, H. M., J. C.Borrero, C. E. Synolakis, and J. Yoo (2006), 2004 Indian Ocean tsunami flow velocity measurements from survivor videos. *Geophysical Research Letters*, *33*, L24605, doi:10.1029/2006GL026784,2006.

Goff, J., W. C. Dudley, M. J. deMaintenon, G. Cain, and J. P. Coney (2006), The largest local tsunami in 20th century Hawaii. *Mar. Geol*., *226*, 65-79.

Goto, C., Y. Ogawa, N. Shuto, and F. Imamura (1997), IUGG/IOC Time Project, Numerical Method of Tsunami Simulation with the Leap-Frog Scheme. *IOC Manuals and Guides*, *35*, 130 pp., UNESCO, Paris.

Goto, K., S. A. Chavanich, F. Imamura, P. Kunthasap, T. Matsui, K. Minoura, D. Sugawara, and H. Yanagisawa (2006), Distribution, origin and transport process of large boulders deposited by the 2004 Indian Ocean tsunami at Pakarang Cape, Thailand, paper presented at 17th International Sedimentological Congress, IAS, Fukuoka, Japan.

Goto, K., F. Imamura, N. Keerthi, P. Kunthasap, T. Matsui, K. Minoura, A. Ruangrassamee, D. Sugawara, and S. Supharatid (2007 accepted), Distributions and significances of the 2004 Indian Ocean tsunami deposits—Initial results from Thailand and Sri Lanka, in *Developments in Sedimentology. Tsunamites—Their features and Implications,* edited by T. Shiki, et al. (eds.), Elsevier, Berlin.

Hoerner, S. F (1965), Fruid Dynamic Drag. pp.3.1-3.28. published by the author.

Imamura, F., I. Yoshida, and A. Moore (2001), Numerical study of the 1771 Meiwa tsunami at Ishigaki Island, Okinawa and the movement of the tsunami stones. *P. Coast. Eng*., *JSCE*, *48*, 346-350.

Julien, P. Y. (1995), Erosion and Sedimentation, 280pp. Cambridge Univ. Press., Cambridge.

Kato, Y., M. Kimura (1983), Age and origin of so-called "*Tsunami-ishi*", Ishigaki island, Okinawa prefecture. *J. Geol. Soc. Japan*, *89*, 471-474.

Kawana, T. (2000), Field guidebook for tsunami disaster prevention. 25pp. Research association for Tokai, To-nankai and Nankai Earthquake Tsunamis, Osaka, Japan.

Kotani, M., F. Imamura, and N. Shuto (1998), Tsunami run-up simulation and damage estimation by using GIS. *P. Coast. Eng*., *JSCE*, *45*, 356-360.

Linsley, R. K. and J. B. Franzini (1979), Water resources engineering. 716 pp. McGraw-Hill, New York.

Mastronuzzi, G. and P. Sanso (2000), Boulders transport by catastrophic waves along the Ionian coast of Apulia (southern Italy). *Mar. Geol*., *170*, 93-103.

Matsutomi, H., T. Sakakiyama, S. Nugroho, M. Matsuyama (2006), Aspects of inundated flow due to the 2004 Indian Ocean tsunami. *Coastal Engineering Journal*, *48*, 167-195.

Nakamura, M. (2006), Source fault model of the 1771 Yaeyama tsunami, Southern Ryukyu Island, Japan, inferred from numerical simulation. *Pure Appl. Geophys*., *163*, 41-54.

Nakata, T. and T. Kawana (1993), Historical and prehistorical large tsunamis in the southern Ryukyu, Japan. Proceedings, IUGG/IOC International Tsunami Symposium, 297-307.

Nakata, T., and T. Kawana (1995), Historical and prehistorical large tsunamis in the southern Ryukyus, Japan, in *Tsunami: Progress in Prediction, Disaster Prevention and Warning*, edited by Y. Tsuchiya and N. Shuto, pp. 211-222, Kluwer Academic Publishers, Netherlands.

Noji, M., F. Imamura, and N. Shuto (1993), Numerical simulation of movement of large rocks transported by tsunamis. Proceedings of IUGG/IOC International Tsunami Symposium, 189-197.

Noormets, R., E. A. Felton, and K. A. W. Crook (2002), Sedimentology of rocky shorelines: 2. Shoreline megaclasts on the north shore of Oahu, Hawaii - origins and history. *Sed. Geol*., *150*, 31-45.

Noormets, R., K. A. W. Crook, and E. A. Felton (2004), Sedimentology of rocky shorelines: 3: Hydrodynamics of megaclast emplacement and transport on a shore platform, Oahu, Hawaii. *Sed. Geol*., *172*. 41-65.

Nott, J. (2000), Records of prehistoric tsunamis from boulder deposits: evidence from Australia. *Sci. Tsunami Hazard*, *18*, 3-14.

Nott, J. (2003), Waves, coastal boulder deposits and the importance of the pre-transport setting. *Earth Planet. Sci. Lett*., *210*. 269-276.

Nott, J. (2004), The tsunami hypothesis –comparisons of the field evidence against the effects, on the Western Australian coast, of some of the most powerful storms on Earth. *Mar. Geol.*, *208*, 1-12.

Okada, K., K. Goto, F. Imamura, T. Shinozaki (2007 accepted), Field observation and the applicability limit of the model for Boulder Transport by the Tsunami (BTT-model) based on the hydraulic experiment. *P. Coast. Eng.*, *JSCE*, *54*.

Scheffers, A., and D. Kelletat (2005), Tsunami relics on the coastal landscape west of Lisbon, Portugal. *Sci. Tsunami Hazard*, *23*, 3-16.

Simkin, T., and R. S. Fiske (1983), *Krakatau, 1883: the volcanic eruption and its effects*. 464 pp, Smithsonian Inst. Press., Washington, D. C.

Takahashi, T., N. Shuto, F. Imamura, and D. Asai (2000), Modeling sediment transport due to tsunamis with exchange rate between bed load layer and suspended load layer. *P. Int. Conf. Coast. Eng.*, *ASCE*, 1508-1519.

Walder, J. S., P. Watts, and C. G. Waythomas (2006), Case study: Mapping tsunami hazards associated with debris flow into a reservoir. *J. Hydraul. Eng.-ASCE*, *132*, 1-11.

Watts, P. (1998) Wavemaker curves for tsunamis generated by underwater landslides. *J. Waterw. Port. C.-ASCE*, *124*, 127-137.

Watts, P. (2000) Tsunami features of solid block underwater landslides. *J. Waterw. Port. C.-ASCE*, *126*, 144-152.

Whelan, F. and D. Kelletat (2005), Boulder deposits on the southern Spanish Atlantic coast: Possible evidence for the 1755 AD Lisbon tsunami? *Sci. Tsunami Hazard*, *23*, 25-38.

Figure Captions

Figure 1. Field photographs of tsunami boulders at (a) Ohama and (b) Inoda in Ishigaki Island, Japan, both of which were transported by the 1771 Meiwa tsunami according to historical documents [*Kawana*, 2000].

Figure 2. Schematic diagrams showing a water tank for conducting hydraulic experiments: (a) Initial condition, (b) generation and run-up of the bore after rapid opening of the gate, and (c) dewatering process during the backwash flow. A block was set in the bottom of the slope. Point A indicates the point at which the current velocity was measured as shown in figure 3.

Figure 3. Measured and calculated current velocities at point A. Backwash flow is indicated using negative value.

Figure 4. (a) Schematic diagram of the block transport process. (b) Initial orientation of the long axis of the rectangular solid block perpendicular and parallel to the current direction.

Figure 5. Measured (error bar: 1σ) and calculated (for constant and variable μ) maximum displacement and the final position for (a) block A, (b) block B, (c) block C, and (d) block D-1.

Figure 6. Measured maximum displacement and the final position of blocks D-1 to D-3 with the long axis orientation (a) perpendicular or (b) parallel to the current.

Figure 7. Schematic diagram showing varying modes of transport for a block during the hydraulic experiment. The mode of transport is (a) sliding or (b) rolling and saltation, depending on the shape and weight of the block as well as on the current velocity.

Figure 8. Diagram showing a relationship between β and $\mu(t)/\mu_0$.

Figure 9. Numerical result for propagation of tsunami wave at Ishigaki Island, Japan [modified after *Imamura et al*., 2001].

Figure 10. Diagram showing the trajectory of the boulder transported by the tsunami at Inoda area in Ishigaki Island. The star marks indicate the locations of measurements of the time

series for elevation of the water level and the current velocity shown in figure 11.

Figure 11. (a) Diagram showing calculated time-series elevation of water level (m). Diagrams showing velocities (m/s) of the current and the boulder in (b) x-direction and (c) y-direction. Eastward and northward are positive in (b) and (c), respectively.

Table 1. Dimension, density and type of the rock constituting the block using hydraulic experiment.

Block	Dimension (cm^3)	Density (g/cm^3)	type of rock
A	3.2×3.2×3.2	1.55	Coral rock
B	1.6×1.6×1.6	1.79	Coral rock
C	3.2×3.2×3.2	2.71	Silicate rock
D-1	1.6×1.6×1.6	2.71	Silicate rock
D-2	3.2×1.6×1.6	2.71	Silicate rock
D-3	4.8×1.6×1.6	2.71	Silicate rock

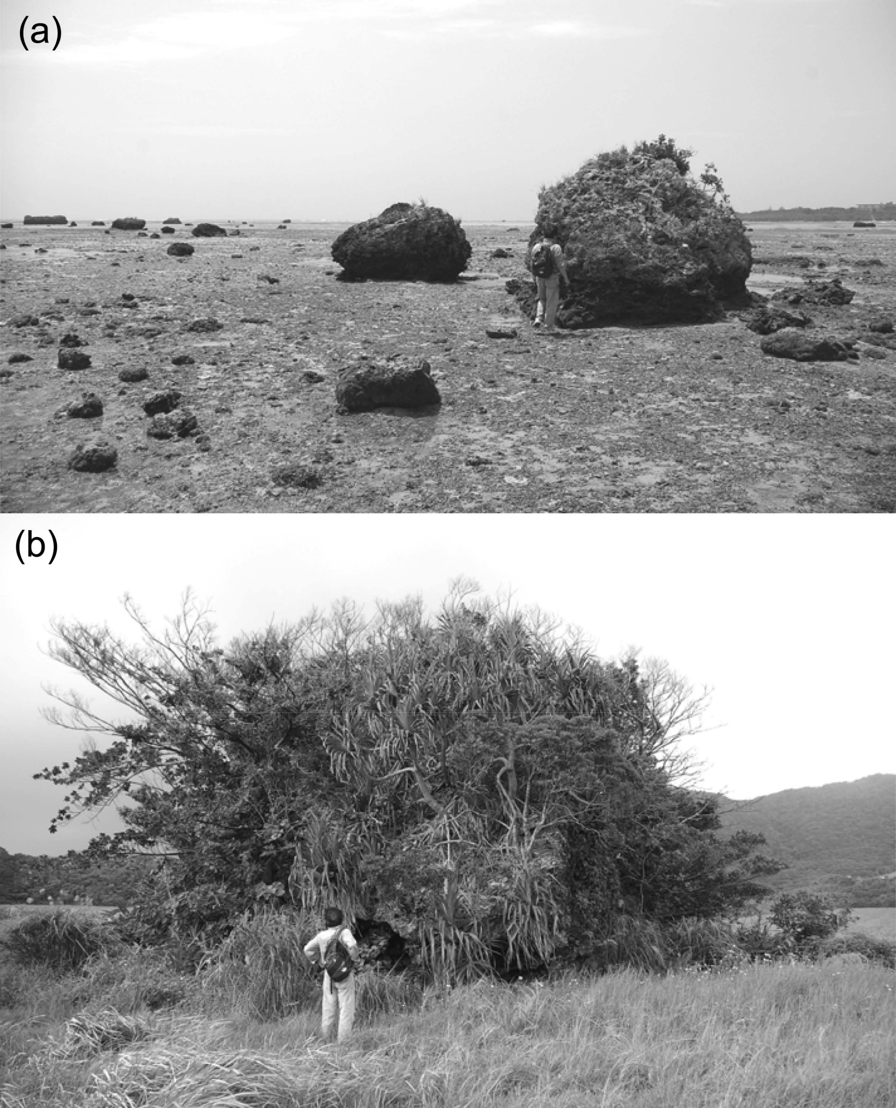
(a)
(b)

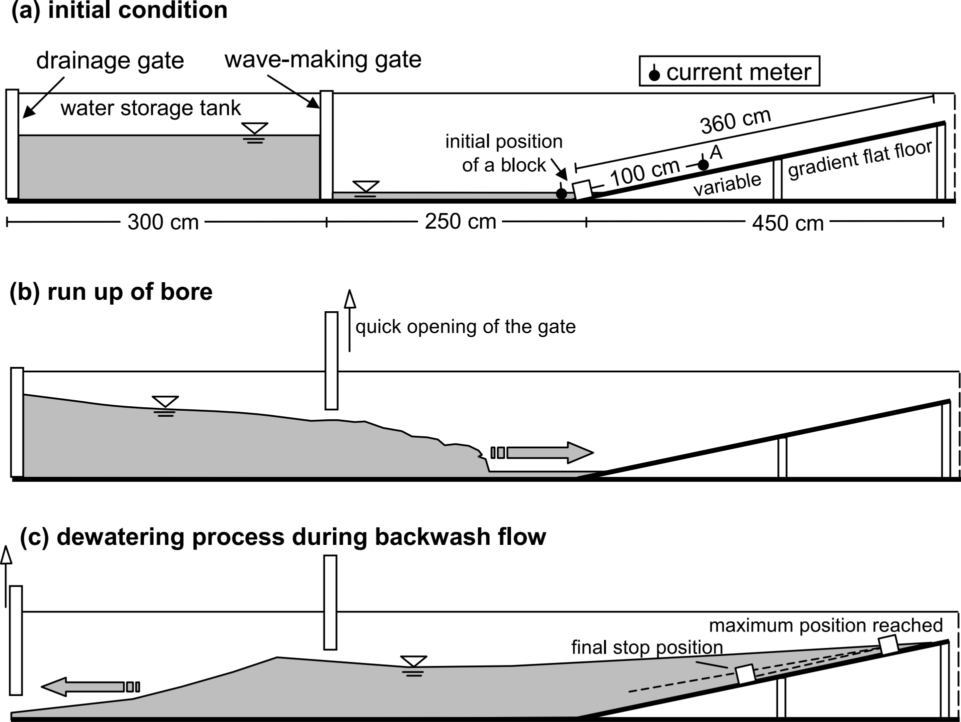

(a) initial condition
drainage gate
wave-making gate
current meter
water storage tank
initial position
of a block
360 cm
A
100 cm
variable
gradient flat floor
300 cm
250 cm
450 cm
(b) run up of bore
quick opening of the gate
(c) dewatering process during backwash flow
maximum position reached
final stop position

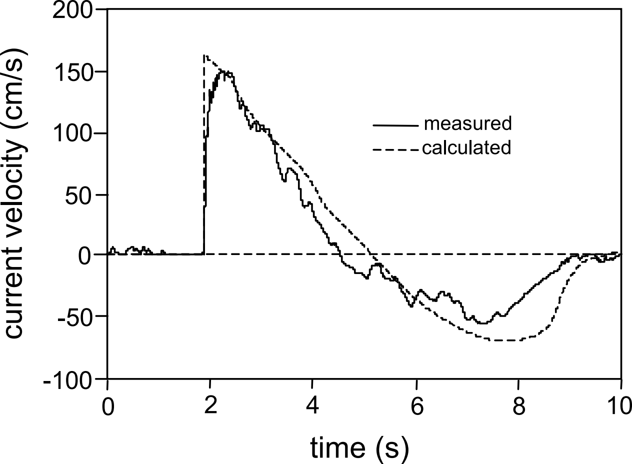

current velocity (cm/s)
200
150
100
50
0
-50
-100
measured
calculated
0
2
4
6
8
10
time (s)

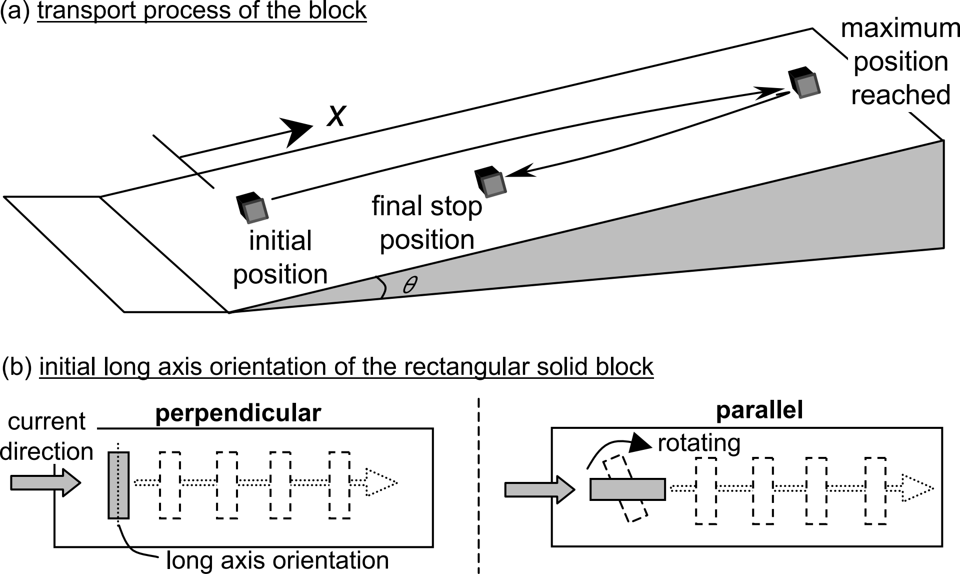

(a) transport process of the block
maximum position reached
x
final stop position
initial position
θ
(b) initial long axis orientation of the rectangular solid block
perpendicular
current direction
long axis orientation
parallel
rotating

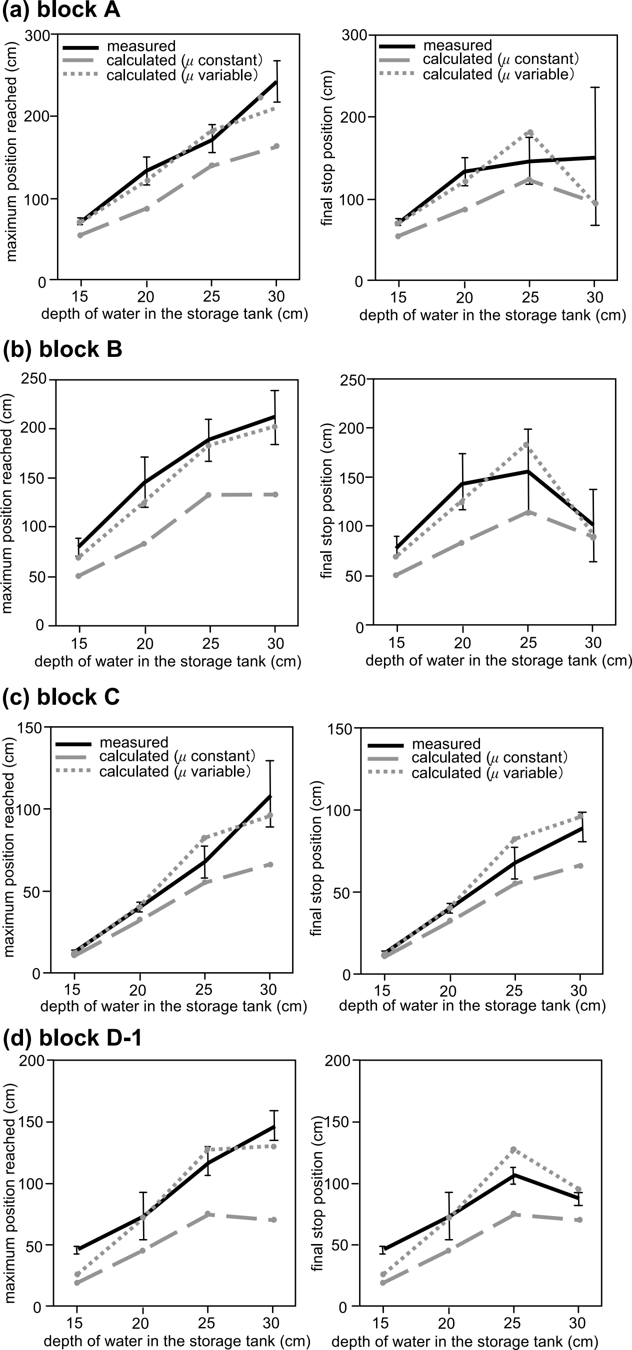

(a) block A
measured
calculated (μ constant)
calculated (μ variable)
maximum position reached (cm)
final stop position (cm)
depth of water in the storage tank (cm)
0
100
200
300
15
20
25
30
(b) block B
maximum position reached (cm)
final stop position (cm)
depth of water in the storage tank (cm)
0
50
100
150
200
250
15
20
25
30
(c) block C
measured
calculated (μ constant)
calculated (μ variable)
maximum position reached (cm)
final stop position (cm)
depth of water in the storage tank (cm)
0
50
100
150
15
20
25
30
(d) block D-1
maximum position reached (cm)
final stop position (cm)
depth of water in the storage tank (cm)
0
50
100
150
200
15
20
25
30

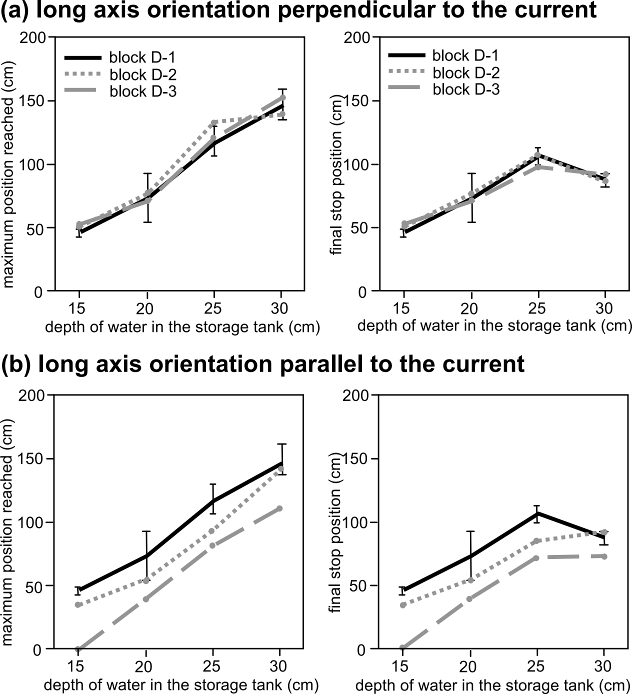
(a) long axis orientation perpendicular to the current
maximum position reached (cm)
block D-1
block D-2
block D-3
depth of water in the storage tank (cm)
final stop position (cm)
block D-1
block D-2
block D-3
depth of water in the storage tank (cm)
(b) long axis orientation parallel to the current
maximum position reached (cm)
depth of water in the storage tank (cm)
final stop position (cm)
depth of water in the storage tank (cm)

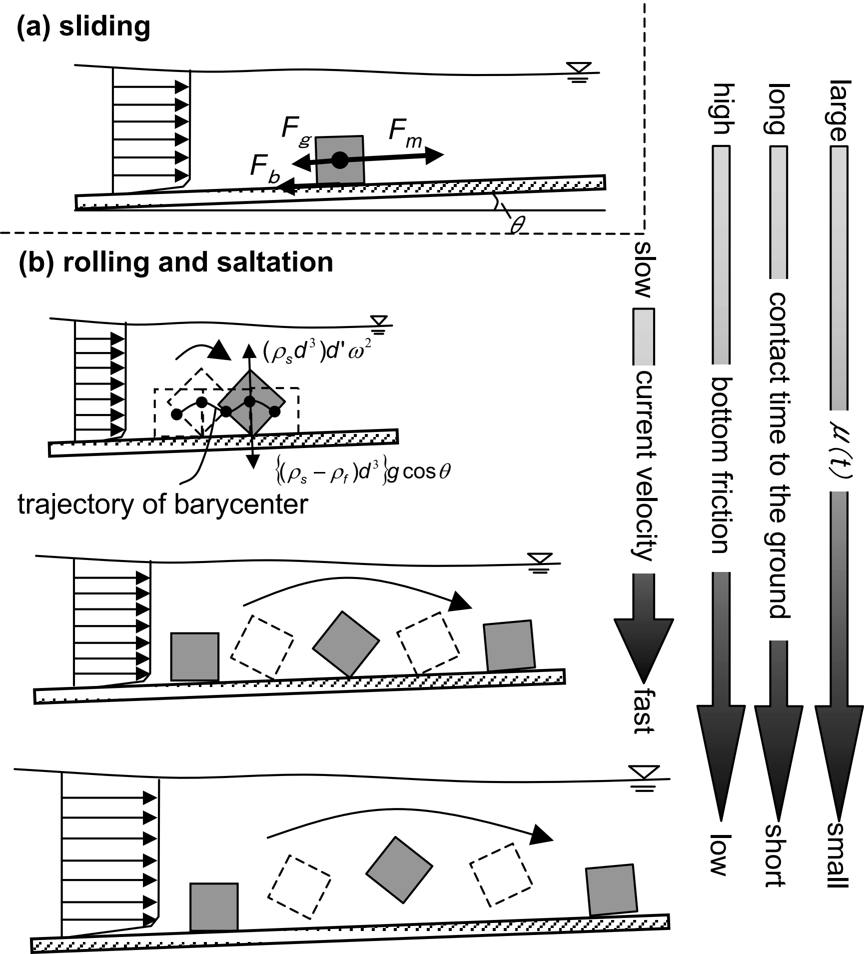
(a) sliding
F_g
F_m
F_b
θ
(b) rolling and saltation
$(\rho_s d^3)d'\omega^2$
$\{(\rho_s-\rho_f)d^3\}g\cos\theta$
trajectory of barycenter
slow
current velocity
fast
high
bottom friction
low
long
contact time to the ground
short
large
$\mu(t)$
small

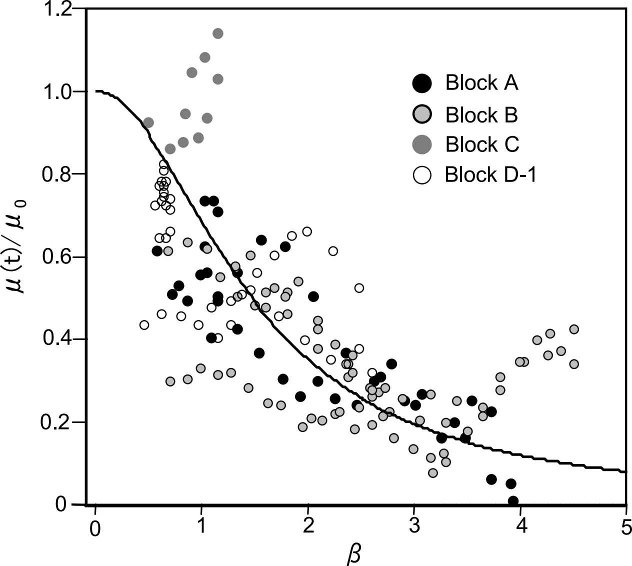

Block A
Block B
Block C
Block D-1
1.2
1.0
0.8
0.6
0.4
0.2
0
0
1
2
3
4
5
μ(t)/μ0
β

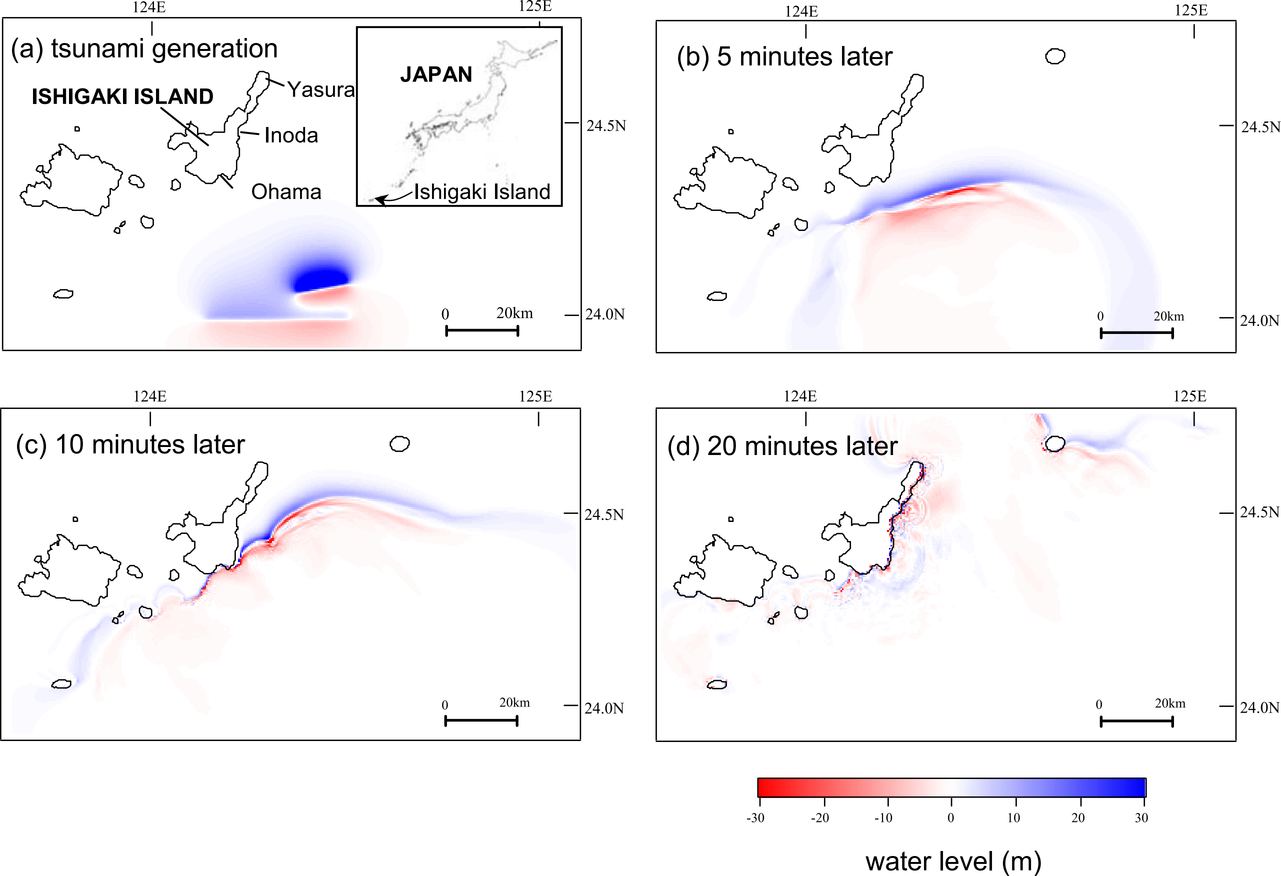

(a) tsunami generation
ISHIGAKI ISLAND
Yasura
Inoda
Ohama
JAPAN
Ishigaki Island
(b) 5 minutes later
(c) 10 minutes later
(d) 20 minutes later
124E
125E
24.5N
24.0N
0
20km
-30
-20
-10
0
10
20
30
water level (m)

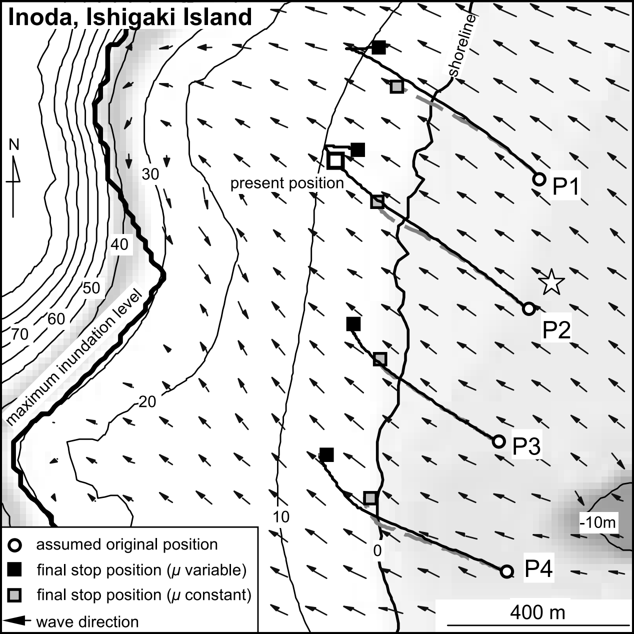

Inoda, Ishigaki Island
N
shoreline
present position
P1
P2
P3
P4
30
40
50
60
70
20
10
0
-10m
maximum inundation level
assumed original position
final stop position (μ variable)
final stop position (μ constant)
wave direction
400 m

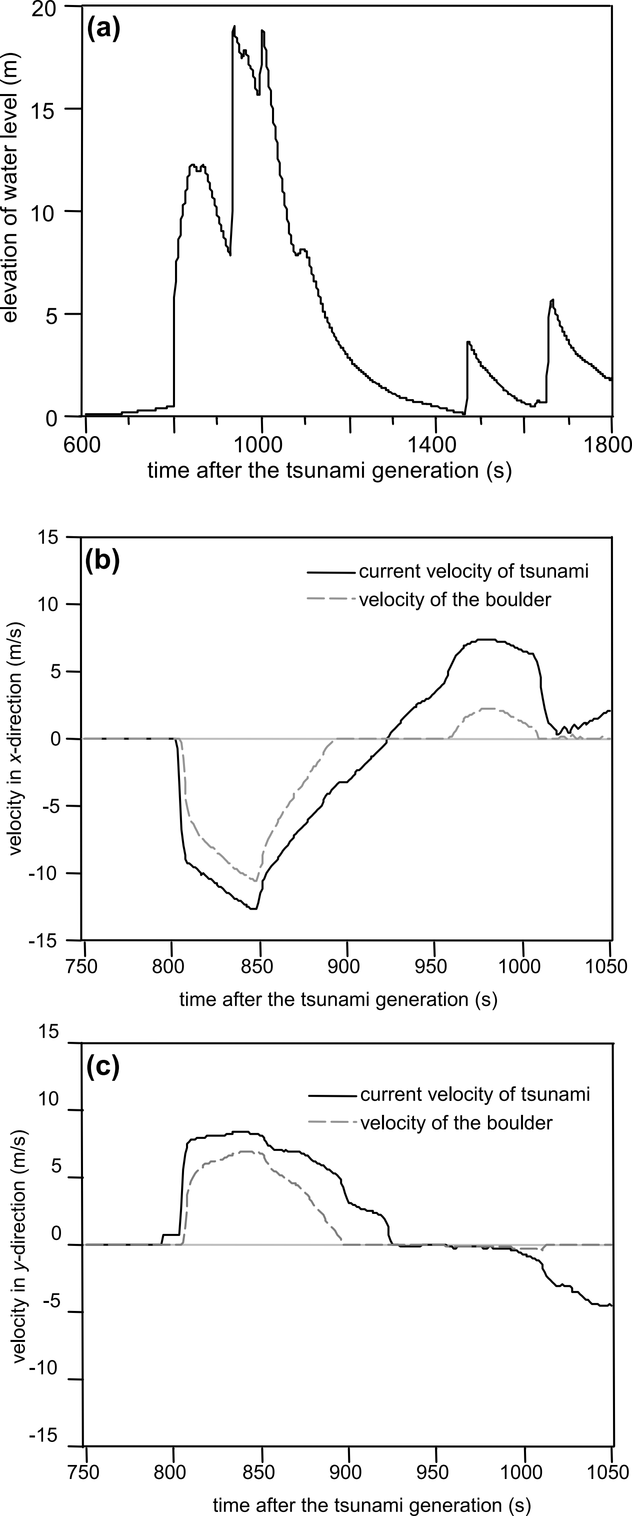
(a)
elevation of water level (m)
0
5
10
15
20
600
1000
1400
1800
time after the tsunami generation (s)
(b)
current velocity of tsunami
velocity of the boulder
velocity in x-direction (m/s)
15
10
5
0
-5
-10
-15
750
800
850
900
950
1000
1050
time after the tsunami generation (s)
(c)
current velocity of tsunami
velocity of the boulder
velocity in y-direction (m/s)
15
10
5
0
-5
-10
-15
750
800
850
900
950
1000
1050
time after the tsunami generation (s)